Computational flowfield analysis of a next generation launcher

Antonio Viviani, Giuseppe Pezzella** and Pietro Catalano****
**Industrial and Information Engineering Department*
Second University of Naples
Via Roma, I-81031 Aversa (CE), Italy
***Analysis and Estrapolation to Flight Lab., Head*
****Fluid Dynamic Modelling, Head*
Italian Aerospace Research Centre
Via Maiorise, I-81043, Italy

Abstract
In this research effort launcher aerodynamic design activities at phase-A level are described. The goal is to address the preliminary aerodynamic data-base of a next generation launch vehicle as input for performances evaluations as well as launcher control and sizing. To this end, different design approaches are addressed as engineering methods and computational fluid dynamics with both Euler and Navier-Stokes approximations.

1. Introduction

During the development phase the launchers' needs for aerodynamic characterization are fulfilled by a hybrid approach encompassing wind tunnel testing (WTT) and computational fluid dynamics (CFD) results [1]. The joint use of WTT and CFD is a powerful tool, able to provide high quality data as input for performances evaluations as well as launcher control and sizing.
Aerodynamics for launcher systems focuses on the assessment of the loads the atmosphere determines over the quick moving and accelerating vehicle. These forces are applied through pressure and friction effects on the external launcher surface, thus resulting in a global aerodynamic force [2].
The assessment of launcher aerodynamic is fundamental for the determination of the launcher's performances and control software. Indeed, in the motion direction, the aerodynamic drag slows the launcher.
On the other hand, the global aerodynamic force generally does not act at vehicle centre of gravity (CoG) location, then the aerodynamic moment exerted at the CoG can lead to stable or unstable behaviour of the launcher, to account for in the launcher's control software. Moreover, launchers structures and protrusions should sustain the aerodynamic loads all along the trajectory. This also should be taken into account in the general loading studies devoted to the launcher sizing. The building of detailed data bases require a very important number of computations, to be produced quickly and at low costs. Then, Efforts for tools developments is kept for the following aspects: computational speed (more massive parallelism); industrialization of tools chains (automated meshing for NS computations). Moreover the need for refined models and experiments appears for more complex physics linked to detailed turbulent flow structures. These phenomena are directly linked to unsteady aerodynamic environment observed on launchers (buffet). They are also directly driving the flow behaviour at the launcher base, even for mean flow values. This flow region remains today the main source of aerodynamic uncertainty before flight. Recent approaches like LES or DES are promising but remain too expansive at full scale for a systematic use.

2. Aerodynamic conventions for launchers

Aerodynamic data for launchers are provided in the body reference frame (BRF) as illustrated in Figure 1 and Figure 2 where:

- V (u,v,w) is the CoG speed relative to air,
- O is the coordinate system reference point (different from the CoG),
- X is the central revolution body axis: directed from O to the nose of the launcher,
- Y is the transverse axis,

• Z is the normal axis built to obtain a direct coordinate system, φ is the roll angle around the X axis,
• Z_ϕ is the transformation of Z by the ϕ rotation around X which contains V,
• α_e is the global incidence of the launcher,
• α is the angle of attack (i.e., the angle between X and V projection in the (X,Z) plane),
• β is the side slip angle (i.e., the angle between V projection in the (X,Z) plane and V).

These conventions come from the ISO norm. 1151 and are exemplified in Figure 1 [1][3].

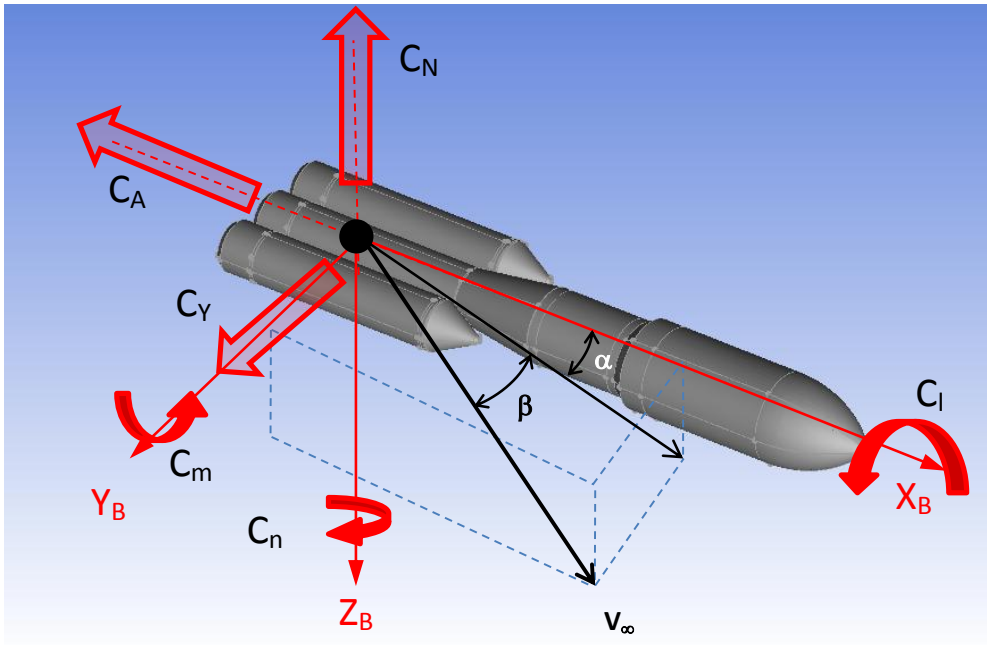

Figure 1 Conventional Body Reference Frame

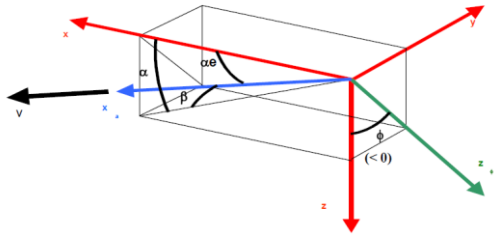

Figure 2 Rear view of the Conventional Body Reference Frame.

The global aerodynamic force $\vec{F}$ and moment $\vec{M}$ acting on the launcher are expressed in BRF as follows:

$$\vec{F} = S_{ref}\, q_\infty \left(-C_A\, \hat{i} + C_Y\, \hat{j} - C_N \hat{k}\right) \quad \textbf{(1)}$$

$$\vec{M} = S_{ref}\, L_{ref}\, q_\infty \left(C_l\, \hat{i} + C_m\, \hat{j} + C_n \hat{k}\right) \quad \textbf{(2)}$$

where:
C_A: Axial force coefficient,
C_Y: Transverse force coefficient,
C_N: Normal force coefficient,
C_l: Rolling moment coefficient,
C_m: Pitching moment coefficient,
Cn: Yawing moment coefficient,
$\left(\hat{i}, \hat{j}, \hat{k}\right)$ are the reference unit vectors
S_{ref}: Reference surface,

L_{ref}: reference length
q_∞: the dynamic pressure.

The definition of force and moment coefficients is:

$$C_i = \frac{F_i}{\frac{1}{2}\rho_\infty v_\infty^2 S_{ref}} \qquad i = L, D \tag{3}$$

$$C_{M_j} = \frac{M_j}{\frac{1}{2}\rho_\infty v_\infty^2 L_{ref} S_{ref}} \qquad j = Y \tag{4}$$

with:

ρ_∞: atmospheric density,
V_∞: speed relative to air.

3. Aerodynamic Coefficients and Vehicle Design

As previously mentioned aerodynamic coefficients are used at system level for the determination of launcher performances and control, as well as for general loading determination.
The launcher control always aims at a null global incidence of the vehicle, except during manoeuvres. As a consequence, performances studies use only the axial force coefficient CA as the aerodynamic force opposing to the movement. This coefficient should be provided as a function of the Mach number, M_∞:

$$C_A = f(M_\infty) \tag{5}$$

For the control software which commonly directs the thrust of nozzles in the proper direction, the main aerodynamic parameter is the evaluation of moment at the CoG location. Due to the fact that propellants are continuously consumed along the flight, the CoG location is continuously changing too. As a consequence, aerodynamic moments are provided at a conventional location. For example, for ARIANE 5 this location is the main stage nozzle's gimbals point. For general loading studies the main input parameters are the distributed aerodynamic forces and moment coefficients. By distributed coefficients we mean integration of pressure forces and moments on the surface from the fairing nose down to prescribed body cross sections of interest for general loading studies.
Pressure and friction contributions are separated because surface measurements of pressure are easily obtained in wind tunnel testing whereas friction is not. Moreover, wind tunnel flow conditions are generally not representative of real flight conditions for friction. Indeed, wind tunnel can reproduce the Mach numbers seen in flight on a scaled launcher model, giving access to representative pressure coefficients, but generally can't reproduce the flight Reynolds number which is necessary to get representative friction contributions. Nevertheless, pressure contributions are the main contributor to the aerodynamic efforts, and generally friction contributions can be neglected except for the axial force [3].

The pressure force, $\vec{F}_p$, acting on the launcher body surface, S, can be expressed as:

$$\vec{F}_p = \int_S \left(p - p_\infty\right) \cdot \vec{n}\, ds \tag{6}$$

where $\vec{n}$ is the local normal to *S*. Thus, the distributed coefficients for force and moment read:

$$\frac{dC\vec{F}_p}{dx}(x) = -\frac{1}{S_{ref}} \int_{C(x)} C_p \cdot \vec{n}\, \frac{ds}{dx} dx \tag{7}$$

$$\frac{dC\vec{M}_p}{dx}(x) = -\frac{1}{S_{ref}\,L_{ref}}\int_{C(x)} C_p \cdot \vec{P}\times\vec{n}\,\frac{ds}{dx}\,dx \qquad \textbf{(8)}$$

where the integral is computed along cut sections, like C on Figure 3:

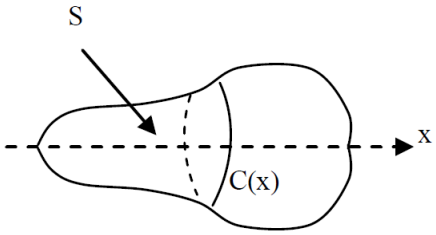

Figure 3: Closed body surface.

This finally gives the global force and moment coefficients:

$$C\vec{F}_p = \int_x \frac{dC\vec{F}_p}{dx}(x)\,dx \qquad \textbf{(9)}$$

$$C\vec{M}_p = \int_x \frac{dC\vec{M}_p}{dx}(x)\,dx \qquad \textbf{(10)}$$

4. Aerodynamic Analysis of Launchers

Classically aerodynamic studies rely on wind tunnel testing and CFD. For launchers the encountered flow regimes begin at null speed on the launch pad and goes up to hypersonic regime in high atmosphere [4].
As far as launcher sizing and control is concerned, it is worth noting that the most sizing part of a launcher trajectory arises when the dynamic pressure is high. As shown in Figure 4, the main part of the needed characterizations is situated in the range $0.5 \leq M_\infty \leq 3$ [1]. Nevertheless, this remains a quite large domain to be covered, encompassing transonic and supersonic regimes [5].

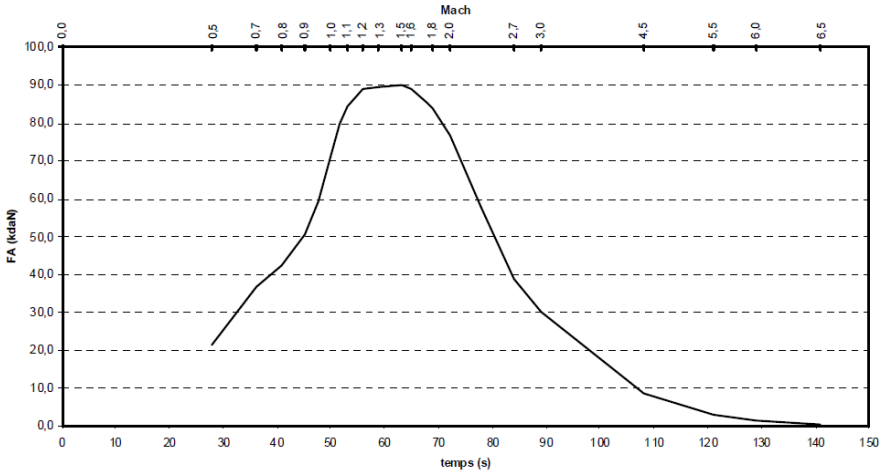

Figure 4 Example of flight domain.

Wing tunnel testing consists generally of two kinds of tests. The first one enables measurement of global aerodynamic coefficients of a launcher model like is illustrated in Figure 5. The model is mounted on a sting equipped with six degrees of freedom balance able to measure each of the six previously defined force and moment

components. Given the Mach number similarity, the calculated force coefficients can represent the full scale's ones. But, wind tunnel test conditions generally do not fully represent flight flow conditions due to different viscous effects as will be detailed further, and complementary use of CFD is very important to reach fine characterization of the aerodynamic shape [3][4][5].

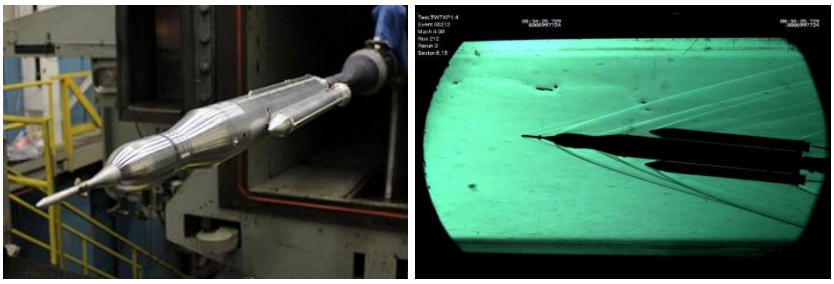

Figure 5 Space Launch System (SLS) Block I vehicle configuration (SLS-1000x) at the Boeing Polysonic Wind Tunnel (PSWT) in St. Louis, Missouri.

The second kind of test is devoted to the measurement of local pressures on the model, which are used to determine sizing for local structures or protrusions as well as the distribution along the launcher of the global aerodynamic coefficients. From these kinds of tests one aims at rebuilding a full mapping of pressure distribution over the launcher, then pressure sensors should be as numerous as possible. A classical method to build the distributed coefficients from wind tunnel testing involves four types of tests: Global weighting with balance for the smooth configuration (without protrusions); Local pressure measurements for the smooth configuration; Global weighting with balance for the full configuration with protrusion; Local pressure measurements for the full configuration with protrusions [6].

Distributed coefficients along x axis for the smooth configuration is obtained with the two first tests. Local pressure measurements can be quite numerous but their number lead to a discretization far less than the one obtained through computation. Then the obtained integration precision is also less. Moreover, even if tests are performed in the same wind tunnel, pressure campaign is not the same as the one for global forces measurements. Then adjustments are performed in order to ensure that distributed coefficients integration gives the measured global coefficients value.

The third testing compared to the first one provides with the global forces due to the addition of protrusions to the launcher.

Generally in the fourth testing, only the main protrusions are equipped with pressure measurements. Once more, the number of available measurements is far less than the number of wall grid points in computations. Moreover, only the protrusions themselves are equipped, then the influence of protrusions presence over the loading distribution on the underlying smooth geometry is neglected. This fourth campaign is used to determine the repartition and magnitude of local loading due to the protrusions. Then hypothesis should be made about integration surfaces around each measurement, as well as about lacking pressure information in high gradients area for example. Obviously, building of distributed loading with wind tunnel data is not as straightforward as for the global coefficients, and more uncertainties have to be taken into account.

4.1 Quick Design approach for external loading characterization

In Phase-A projects the work is based on quick conception loops between performances, staging, propulsion, aeroshape design and conception, aerodynamics loading and control. For Mach numbers ranging from 0.5 up to 10, aerodynamic characterization of the launcher shape should provide with a database (AEDB) giving:

$$C_A = f(M_\infty)$$

$$\left.\frac{C_N}{d\alpha}\right|_{\alpha=0°} = f(M_\infty) \qquad \textbf{(11)}$$

$$\left.\frac{C_m}{d\alpha}\right|_{\alpha=0°} = f(M_\infty)$$

Spatial derivatives in the axial direction of the previous quantities.

This AEDB should be built quickly and for a lot of launcher variants which are initially envisaged. Order of magnitude for a database building duration is one or two weeks during which tens of computation points should be produced. These needs imply work processes with high level of tools chains automation (meshing, computing, post-processing). Aerodynamic sensitivity studies related to the geometry can be added (shape design with CFD for example for tail planes). Today these studies are performed before wind tunnel testing and are the reference used for concepts selection (i.e., launcher trade-off design).
This approach makes wide use of high performance computers, using meshes made of millions cells for each computation and managing several computation cases in parallel. One key necessary feature is the automated generation of meshes for each computation case, without which the allocated timeframe would not be sustainable.
In order to get reasonable quality of results meshes are adapted for each Mach number in order to adequately fit each region with important gradients like compression, shocks and expansion. Best compromise for precision versus number of grid cells is generally obtained with hexahedra cells.
Nevertheless, building multiblock structured or hybrid grids is quite an important constraint for this type of complex topologies. Then, using fitted grid for each Mach number computations are submitted in parallel on several computers, each computation being also performed in parallel mode on several processors. Post treatment of each computation is also standardized and automated in order to get quickly a synthetic AEDB.

4.2 The Next Generation Launcher Vehicle (NGLV)

An example of aerodynamic analysis of a next generation expendable launcher by means of CFD is provided hereinafter. The aeroshape under investigation features two boosters and a central core stage with hammerhead fairings, see Figure 6. It is close to that expected for ARIANE 6 concept being developed by European Space Agency.

Figure 6 The NGLV aeroshape.

Launcher aerodynamics has been addressed considering four Mach numbers, namely 0.5, 1.1, 2.5, and 5, at three angle of attacks, i.e., α=0, 5, and 7 deg, as shown in Table 1. Therefore, Eulerian and Navier-Stokes 3-D CFD computations have been carried out on several unstructured hybrid meshes.

Table 1 The CFD Test Matrix

	Mach			
AoA, deg	0.5	1.1	2.5	5
0	E	E	E	E
5	E	E	E, NS	E, NS
7	E	E	E	E

E: Eulerian CFD
NS: Navier-Stockes CFD

An overview of the unstructured mesh domain at M_∞=0.5 is shown in Figure 7 (left side), where the grid in the launcher symmetry plane is provided. A blow-up of the mesh close and over the launcher is also provided.

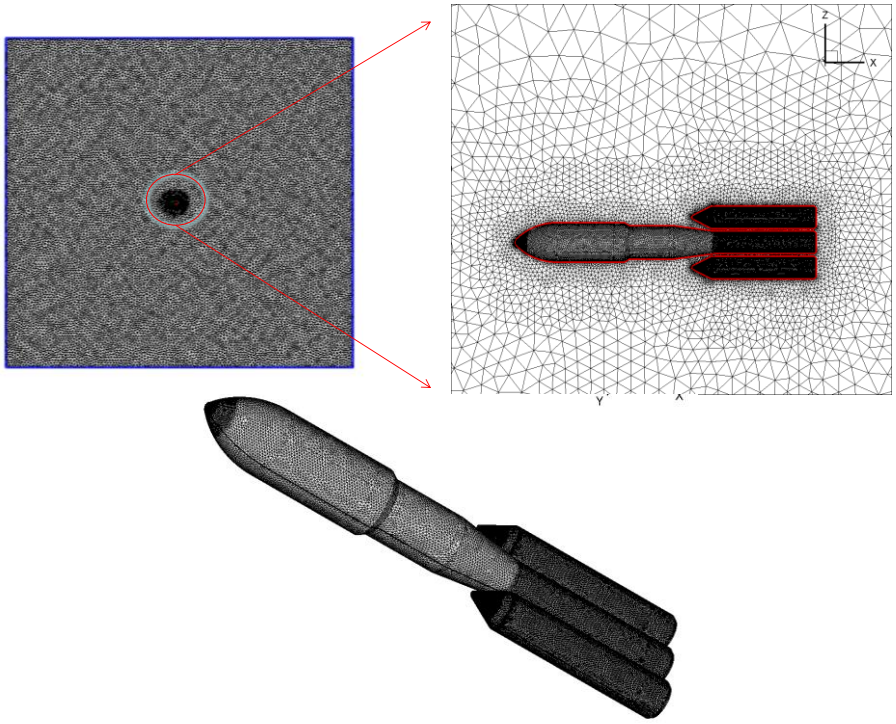

Figure 7 Overview of the unstructured mesh domain at M_∞=0.5 and α=0 deg.

As on can see, a square brick wide twenty body length upstream, downstream, upward and downward the launcher to assure farfield unperturbed flow conditions is considered. Indeed, in a subsonic (i.e., flow moving slower than the speed of sound) elliptic flow disturbance due to the body are propagated upstream via molecular collisions at approximately the speed of sound, thus influencing flow everywhere, see Figure 8. Therefore, the computational domain must be wide enough to avoid interferences between flowfield and farfield boundary conditions.

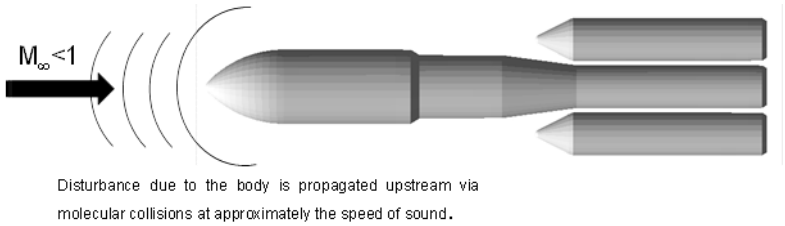

Figure 8 Propagation of disturbance in subsonic flow

The pressure distribution expected on the surface of launcher flying at M_∞=0.5 and α=5 deg is provided in Figure 9

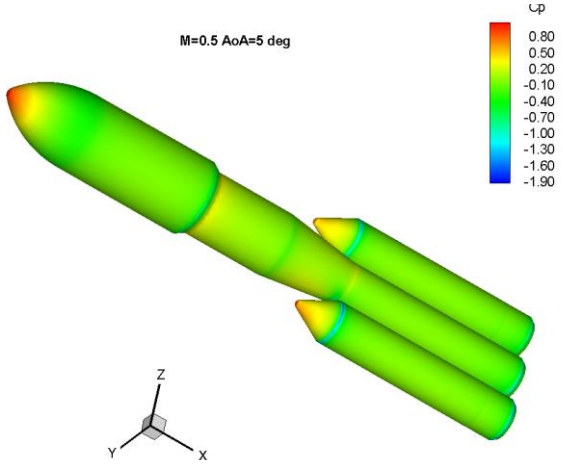

Figure 9 Pressure coefficient at M_∞=0.5 and α=5 deg. Eulerian flow conditions (see Table 1).

Flow compression at stagnation region of launcher fairings and of booster conical forebodies is clearly shown. A recompression zone at the beginning of the cylindrical trunk, just after the fairings, and on that close to the booster forebodies can be also noted. Numerical investigations at higher Mach number, say M_∞=2.5, have been performed on a narrow grid domain compared to that in Figure 7. An overview of surface mesh on launcher symmetry plane and surface is provided in Figure 10.

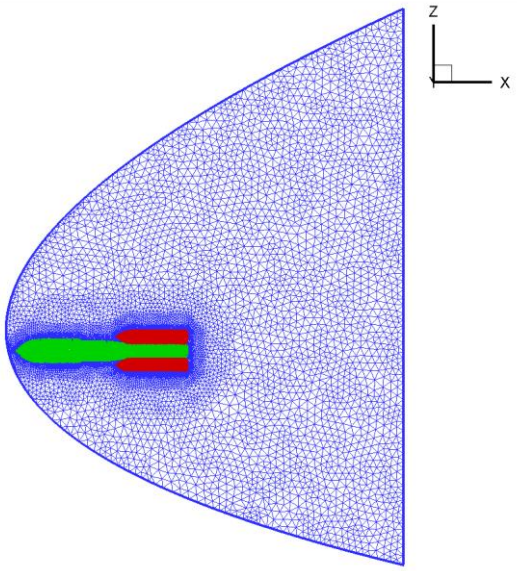

Figure 10 Overview of the unstructured mesh domain at M_∞=2.5 and α=5 deg.

Indeed, at supersonic speed a shock wave appears at launcher leading edge (i.e., hyperbolic flowfield) because of when flow moves faster than the speed of sound, disturbances cannot work their way upstream. As a results, disturbances coalesce forming a standing wave, namely bow shock (see Figure 11).

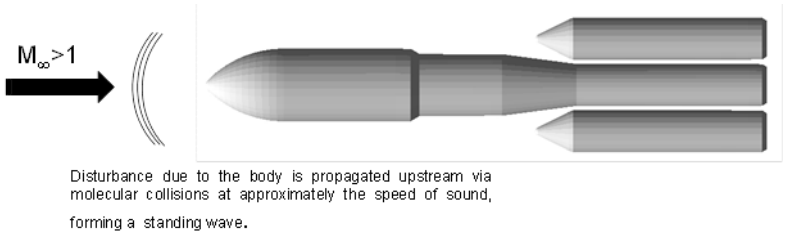

Figure 11 Propagation of disturbance in supersonic flow.

The bow shock that takes place when the launcher flies at M_∞=2.5 and α=5 deg is shown in Figure 12, where Mach number field is provided on vehicle symmetry plane and pressure coefficient contours on launcher surface. The CFD computation is carried out with SST k-ω turbulence flow model and for cold wall boundary condition.
Figure 12 highlights also a complex flowfield past the launcher. For instance, after compression at conical flare of the fairings the flow undergoes to expansions that aligns it along with the constant cross section part of fairing. Hence, at the end of fairings another strong expansion takes place to accommodate the flow to the variation in launcher cross section (i.e., narrow cross section due to fairing boat-tail). Then, a shock wave arises at the beginning of the cylindrical trunk, just after the fairings, to redirect the flow along with the launcher wall. Flow complexity increases further in the region close to the boosters. Here, complex shock-shock and shock-wave boundary layer interactions take place. They result in higher thermo-mechanical loads (i.e., pressure and thermal overshoots) on the launcher wall that must be carefully addressed in vehicle design.
An overview of pressure coefficient distribution on launcher symmetry plane and surface at M_∞=2.5 and α=5 deg, with streamtraces, is provided in Figure 13.

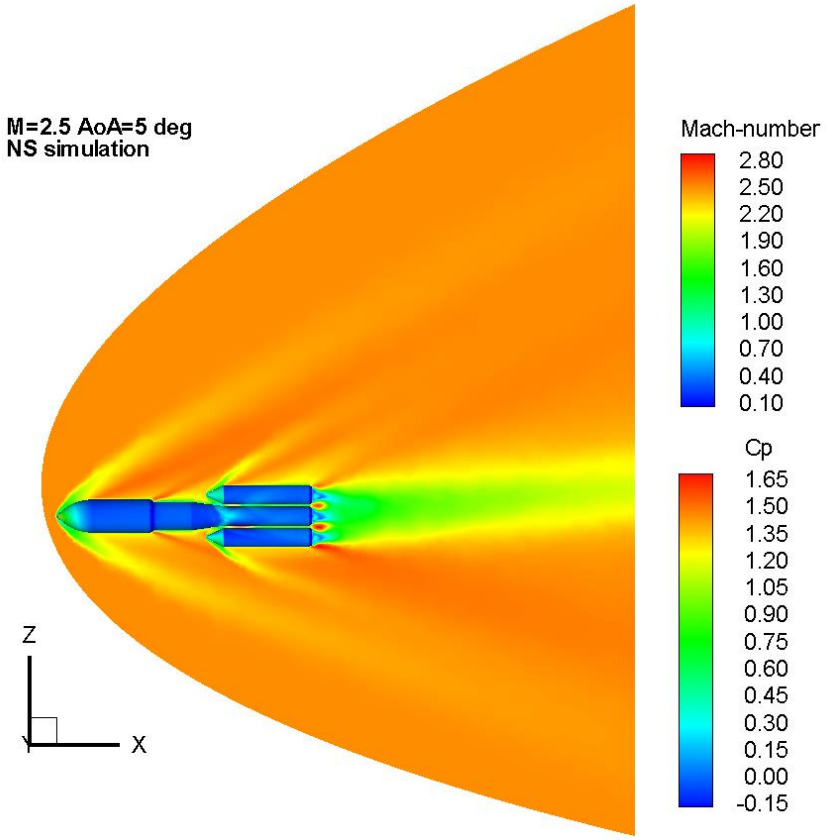

Figure 12 Mach number field on symmetry plane and Cp on launcher surface at M_∞=2.5 and α=5 deg.

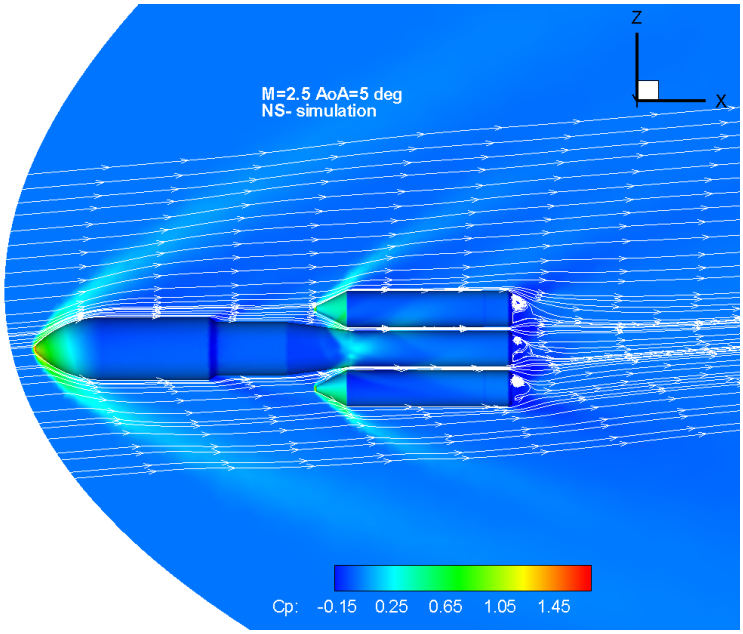

Figure 13 Overview of Cp distribution on symmetry plane and launcher at M_∞=2.5 and α=5 deg, with streamtraces.

The flowfield past the launcher at higher Mach and AoA is shown in Figure 14, where Mach number field on symmetry plane and pressure coefficient on launcher surface at M_∞=5 and α=7 deg are provided. The effect of AoA is clearly evident in the Mach number field past the launcher. As far as aerodynamic coefficients are concerned, NGLV axial force, normal force and pitching moment coefficients are summarized from Figure 15 to Figure 20.

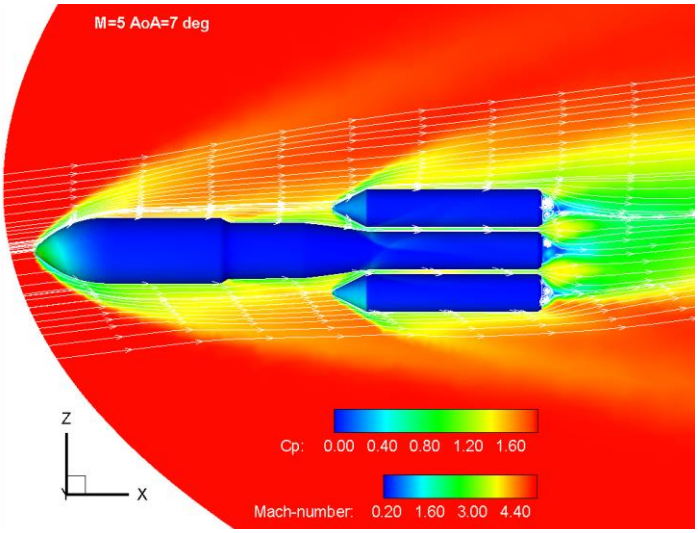

Figure 14 Mach contours distribution on symmetry plane and pressure on launcher at M_∞=2.5 and α=5 deg.

For instance, C_A, C_N, and C_m versus AoA are shown in Figure 15, Figure 16, and Figure 17, respectively; while Figure 18, Figure 19, and Figure 20 report the same coefficients but as function of Mach number. Looking at the axial force coefficient, Figure 15 points out that the CA does not significantly change passing from 0 to 7 deg AoA at each considered Mach number; while the effect of flow compressibility is remarkable, as shown in Figure 18.

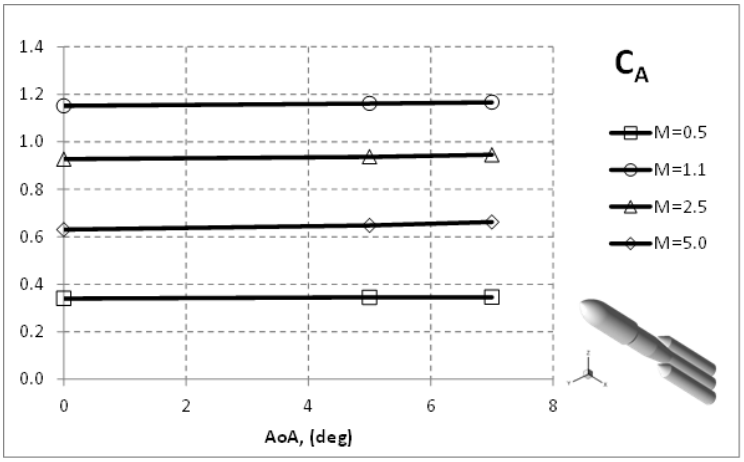

Figure 15. Axial force coefficient versus AoA at different Mach numbers.

Regarding normal force coefficient numerical results in Figure 16 highlight that, for each Mach number, C_N features a quite linear slope as α increases up to 7 deg AoA.

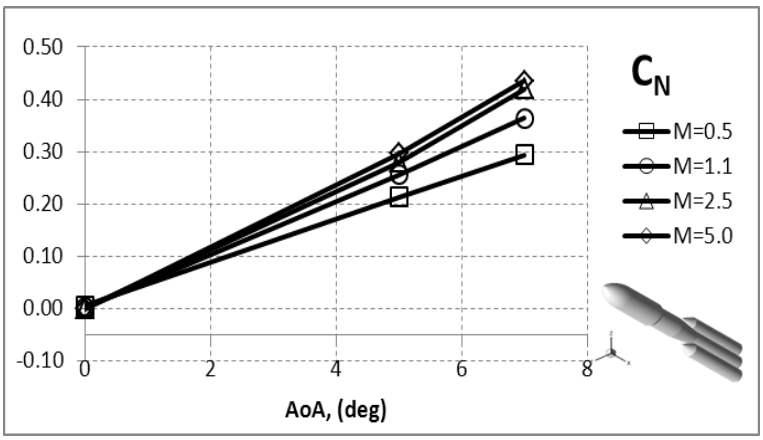

Figure 16 Normal force coefficient versus AoA at different Mach numbers.

Also in this case, compressibility effect influences NGLV normal force by means of different curve slopes for each Mach number case (see Figure 19).
Finally, the vehicle pitching moment coefficient (see Figure 17) features a behaviour quite close to that described for the C_N with a strong pitch down detected for M_∞=5.

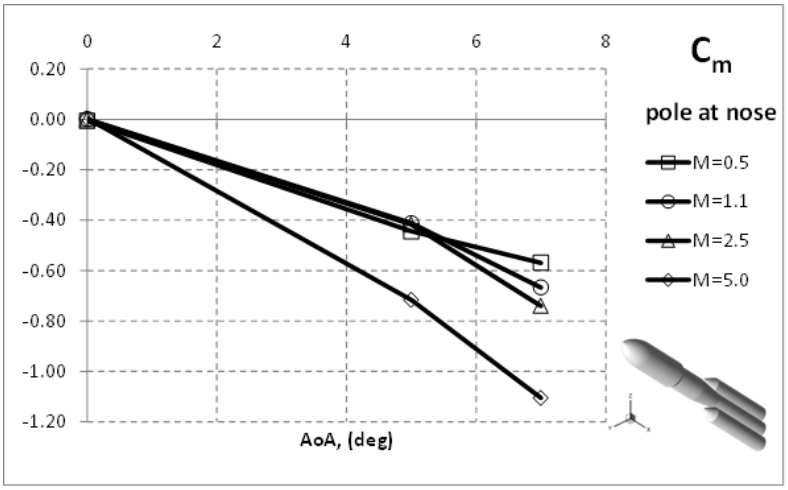

Figure 17 Pitching moment coefficient versus AoA at different Mach numbers.

Profiles of C_A in Figure 18 underline the strong increase to which undergoes the axial aerodynamic force when M_∞ ranges from 0.5 to 5.

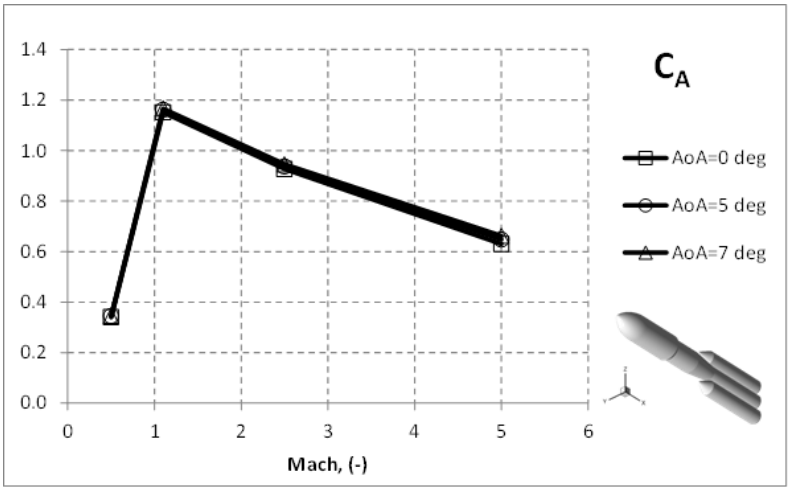

Figure 18 Axial force coefficient versus Mach at different AoA.

Indeed, once Mach number crosses a critical value a shock wave appears in front of launcher, as described in Figure 11. As a result, a new contribution to vehicle aerodynamic drag must be accounted, namely wave drag. This contribution tend to be less strong as Mach number goes towards hypersonic speed conditions considering that the shock becomes weak due to the streamlined vehicle aeroshape (i.e., high inclined shock to assure a narrow shock layer). This determines the classical peak shape of CA versus M_∞, summarized in Figure 18. In particular, all curves are very close each other, as suggested by Figure 15.

The variation of C_N and Cm in Figure 19 and Figure 20 suggest, also on these coefficients, the influence of flow compressibility even in a weaker way. In particular, both C_N and Cm at α=0 deg are zero due to the symmetric launcher aeroshape.

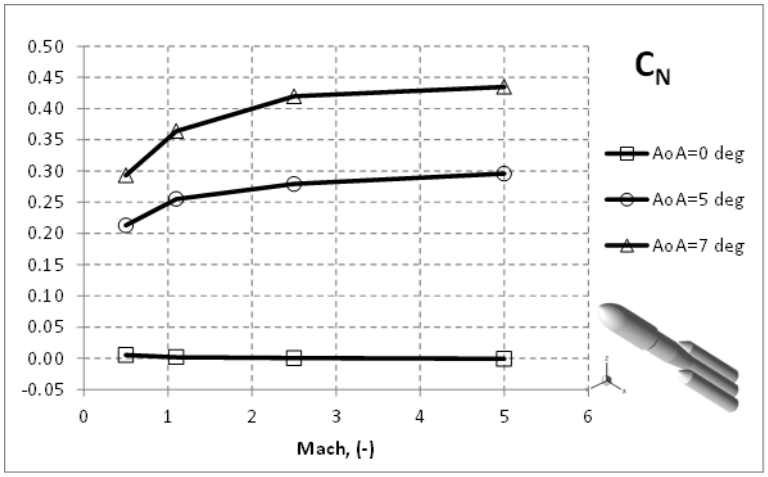

Figure 19 Norma force coefficient versus Mach at different AoA.

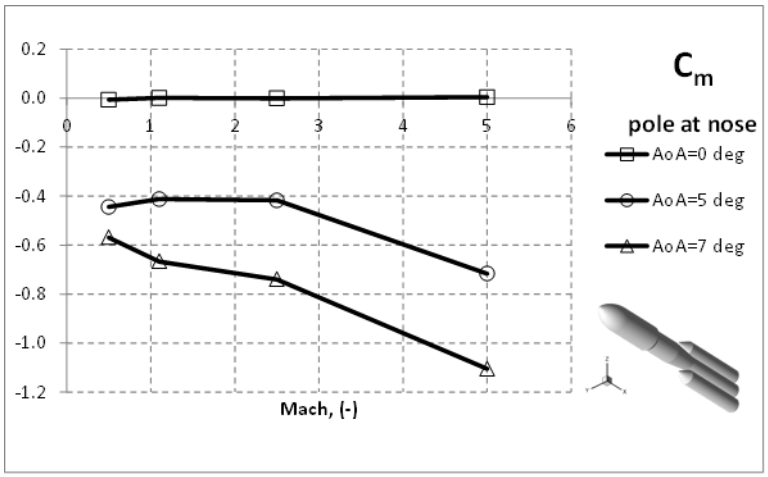

Figure 20 Pitching moment coefficient versus Mach at different AoA.

5. Concluding Remarks

In this research effort launcher aerodynamic design activities at phase-A level are described. The goal is to address the preliminary aerodynamic data-base of a next generation launch vehicle as input for performances evaluations as well as launcher control and sizing. To this end, computational fluid dynamics, with both Euler and Navier-Stokes approximations, are addressed considering four Mach numbers, namely 0.5, 1.1, 2.5, and 5, at three angle of attacks, i.e., α=0, 5, and 7 deg,. For this test matrix launcher aerodynamic performance in terms of axial, normal and pitching moment coefficients is provided. Numerical results point out that the axial force coefficient does not significantly change passing from 0 to 7 deg angle of attack at each considered Mach number; while the effect of flow compressibility is remarkable. Regarding normal force coefficient results highlight that, for each Mach number, it features a quite linear slope as the angle of attack increases up to 7 deg. Finally, the vehicle pitching moment coefficient features behaviour quite close to that described for the normal force coefficient, but a strong pitch down is detected for Mach 5.

References

[1] Pallegoix JF (2014) Launcher aerodynamics. STO-EN-AVT-206
[2] Antonio Viviani and Giuseppe Pezzella, Next Generation Launchers Aerodynamics. Research Signpost, T.C. 37/661 (2), Fort P.O., Trivandrum-695 023. Kerala, India. ISBN: 978-81-308-0512-2
[3] Antonio Viviani and Giuseppe Pezzella, Aerodynamic and Aerothermodynamic Analysis of Space Mission Vehicles. Springer International Publishing. DOI: 10.1007/978-3-319-13927-2. Hardcover ISBN 978-3-319-13926-5. eBook ISBN: 978-3-319-13927-2.

[4] Bertin John J. Hypersonic Aerothermodynamics. AIAA Education Series. 1994.
[5] Anderson, J. D., Hypersonic and High Temperature Gas Dynamics, McGraw-Hill Book Company, New York, 1989.
[6] G. Pezzella, M. Marini, P. Roncioni, J. Kauffmann, C. Tomatis. Preliminary Design of Vertical Takeoff Hopper Concept of Future Launchers Preparatory Program. Journal of Spacecraft and Rockets 2009. ISSN 0022-4650 vol.46 no.4 (788-799) doi: 10.2514/1.39193.